# Ni-Catalyzed Cleavage of Aryl Ethers in the Aqueous Phase

Jiayue He, Chen Zhao,* and Johannes A. Lercher*

Department of Chemistry and Catalysis Research Center, Technische Universität München, 85747 Garching, Germany

S *Supporting Information*

ABSTRACT: A novel Ni/SiO$_2$-catalyzed route for selective cleavage of ether bonds of (lignin-derived) aromatic ethers and hydrogenation of the oxygen-containing intermediates at 120 °C in presence of 6 bar H$_2$ in the aqueous phase is reported. The C−O bonds of α-O-4 and β-O-4 linkages are cleaved by hydrogenolysis on Ni, while the C−O bond of the 4-O-5 linkage is cleaved via parallel hydrogenolysis and hydrolysis. The difference is attributed to the fact that the C$_{aliphatic}$−OH fragments generated from hydrolysis of α-O-4 and β-O-4

linkages can undergo further hydrogenolysis, while phenol (produced by hydrolysis of the 4-O-5 linkage) is hydrogenated to produce cyclohexanol under conditions investigated. The apparent activation energies, $E_a(\alpha$-O-4$) < E_a(\beta$-O-4$) < E_a(4$-O-5$)$, vary proportionally with the bond dissociation energies. In the conversion of β-O-4 and 4-O-5 ether bonds, C−O bond cleavage is the rate-determining step, with the reactants competing with hydrogen for active sites, leading to a maximum reaction rate as a function of the H$_2$ pressure. For the very fast C−O bond cleavage of the α-O-4 linkage, increasing the H$_2$ pressure increases the rate-determining product desorption under the conditions tested.
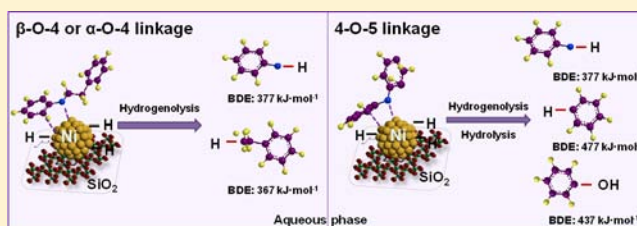
INTRODUCTION

Lignin is a three-dimensional, highly branched, polyphenolic substance containing an array of hydroxy- and methoxy-substituted phenylpropane units.[1] As lignin makes up 20−30 wt % of lignocellulose and especially contains a very high fraction of its energy content (i.e., ca. 40% in the total lignocellulosic biomass[2]), its conversion to energy carriers has recently received much attention. However, because of the high strength and stability of its aryl ether bonds (see Figure 1), selective depolymerization of lignin into small molecules is challenging.[3]

Recently, a series of interesting molecular catalysts, including Ru,[4] V,[5] and Ni[6] complexes, has shown high selectivity in cleaving the C−O bonds of dimeric lignin model compounds to produce aromatic molecules in organic solvents (CD$_3$CN, toluene, and *m*-xylene) under rather mild conditions (80−135 °C, 1 bar H$_2$). In principle, molecular catalysts are logical choices for depolymerization fo lignin, as their mobility and flexibility appear to allow them to reach individual ether bonds without high steric limitation. However, these reported molecular catalysts are sensitive to large concentrations of water, which is costly to separate from raw biomass.

More robust solid catalysts would therefore be better choices for the aqueous-phase conversion of lignin. The strategies explored to date using heterogeneous catalysts such as Ni/ K$_2$CO$_3$/ZrO$_2$, however, require high temperatures (240−400 °C) and pressures (250−315 bar) to cleave the aromatic ethers of lignin dissolved in the aqueous phase.[7] The achievable yields of the cleaved products were limited by recombination of the products via free radical reactions, even when a large excess of H$_2$ was present. Thus, the higher reactivity of the potential products necessitates that the reactions be carried out under very mild conditions. Ni supported on zeolite HZSM-5 showed

appreciable rates of conversion and high stability for hydro-deoxygenation of ethers under moderate conditions (250 °C and 50 bar H$_2$).[8] Similarly, it was shown for Pd-based catalysts that having acid sites in the proximity of the metal sites led to high selectivity for hydrodeoxygenation of substituted phenols.[9] Combining this insight with the finding that Ni molecular catalysts can hydrogenolyze aromatic ether bonds,[6] we chose to explore systematically the properties of supported Ni in the absence of adjacent acid sites on the solid support under much milder conditions.

The representative fragment structure of hardwood lignin depicted in Figure 1 illustrates that the β-O-4, α-O-4, and 4-O-5 linkages are three of the most frequent types of C−O bonds, contributing to 45−62% (the most abundant), 3−12%, and 4−9% of the ether bonds in hardwood lignin, respectively, and would thus be expected to determine the primary products when large clusters of lignin are depolymerized.[10] 2-Phenylethyl phenyl ether, benzyl phenyl ether, and diphenyl ether were selected as model compounds for the β-O-4, α-O-4, and 4-O-5 linkages, respectively, in our exploration of the reaction mechanism of C−O bond cleavage in the aqueous phase, as our previous experiments have shown that more complex substitutions hardly influence the principal chemistry.[11] Here we show that supported Ni catalysts can selectively and quantitatively cleave C−O bonds in aromatic ethers such as benzyl phenyl ether (α-O-4 linkage), 2-phenylethyl phenyl ether (β-O-4 linkage), and diphenyl ether (4-O-5 linkage) to form smaller aromatic molecules, cycloalkanes, and cyclo-
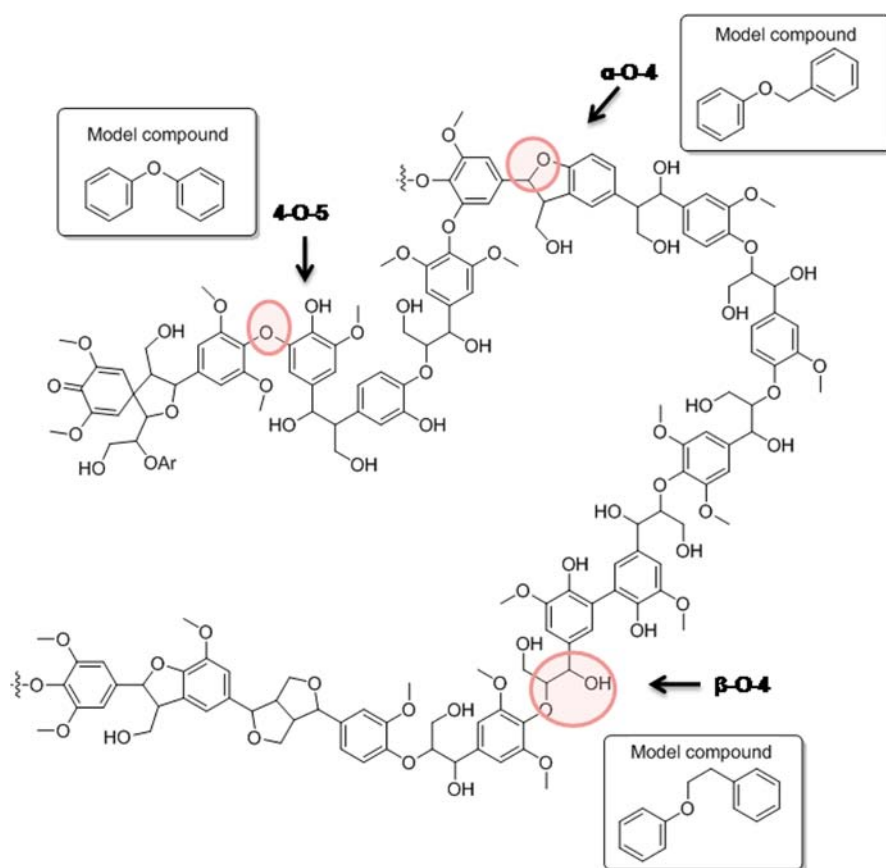
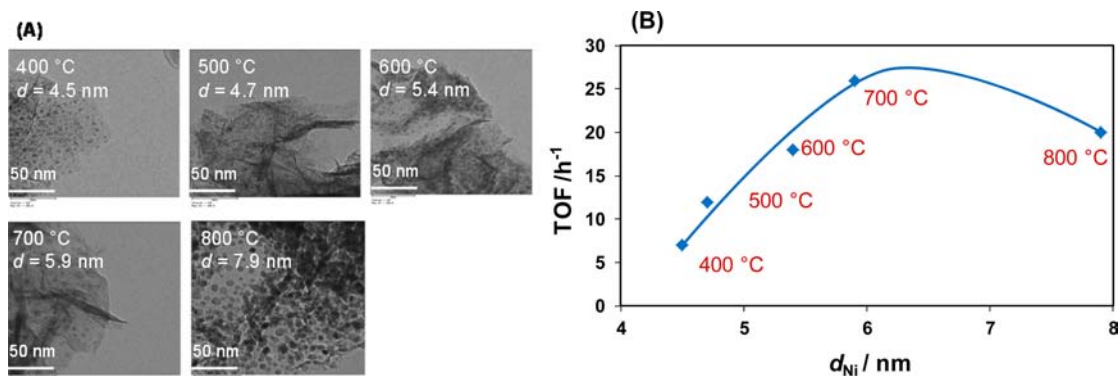**Figure 1.** Fragment structure of hardwood lignin.

Figure 2. (A) TEM images of Ni/SiO$_2$ catalysts prepared by the DP method at different calcination temperatures. (B) TOF as a function of Ni particle size for C–O bond cleavage of 2-phenylethyl phenyl ether (β-O-4) over Ni/SiO$_2$ in water at 120 °C under 6 bar H$_2$.

Table 1. Conversion of 2-Phenylethyl Phenyl Ether (β-O-4) Using Ni/SiO$_2$ Catalysts in Water^a

$T_{calcin.}$ (°C)	Ni loading (wt %)	d_{Ni} (nm)^b	TOF (h^{-1})^c	conv. (%)	selectivity (%)			
					ethylbenzene	cyclohexanol	cyclohexanone	phenol
400	42	4.5	7	5.6	51	18	4.1	27
500	41	4.7	12	12	55	25	2.3	18
600	42	5.4	17	18	50	29	2.1	19
700	46	5.9	26	21	56	31	2.0	11
800	42	7.9	20	8.1	52	19	3.1	26

^{a}Conditions: β-O-4 (1.98 g), Ni/SiO$_2$ (0.30 g), H$_2$O (80 mL), 120 °C, 6 bar H$_2$, 90 min, stirring at 700 rpm. ^{b}Ni particle sizes as determined by TEM. ^{c}The TOFs were normalized by the fractions of accessible Ni atoms on the surface, which were measured by H$_2$ chemisorption to be 0.050, 0.057, 0.051, 0.040, and 0.021 for the Ni/SiO$_2$ samples calcined at increasing temperatures. The reaction conditions were chosen to allow determination of the rate below 20% conversion.
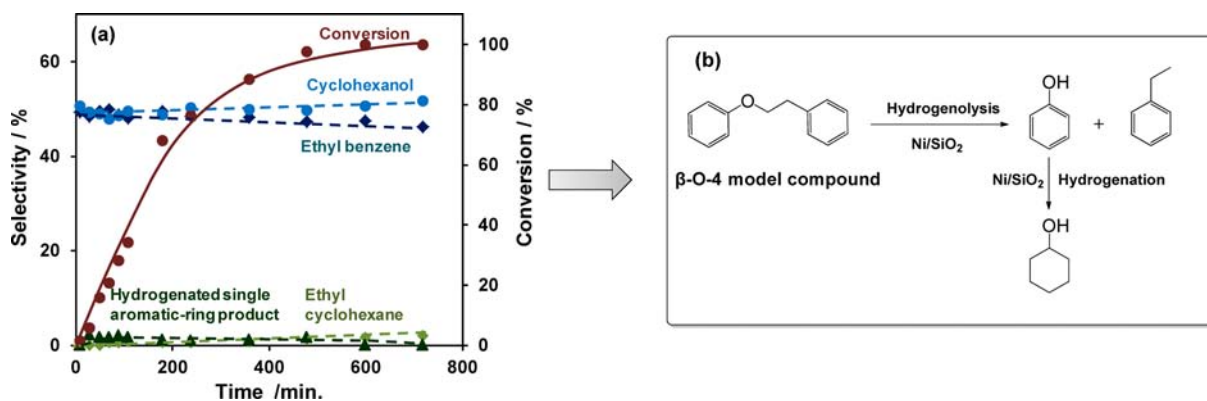
Figure 3. (a) Product distributions for the conversion of 2-phenylethyl phenyl ether (β-O-4) over Ni/SiO$_2$ as functions of time. Reaction conditions: 2-phenylethyl phenyl ether (β-O-4) (1.98 g, 0.010 mol), 57 wt % Ni/SiO$_2$ (0.30 g, 2.91 × 10^{-3} mol of Ni), H$_2$O (80 mL), 120 °C, 6 bar H$_2$, stirring at 700 rpm. (b) Reaction pathway for the cleavage of 2-phenylethyl phenyl ether (the model compound for the β-O-4 linkage in lignin) over Ni/SiO$_2$ in the aqueous phase.

hexanol under very mild conditions (120 °C and 6 bar H$_2$) in water.

■ RESULTS AND DISCUSSION

Catalyst Synthesis Strategy and Catalytic Measurements. We synthesized five supported Ni/SiO$_2$ catalysts using the deposition precipitation (DP) method with urea as the hydrolysis agent. The synthesized Ni/SiO$_2$ catalysts had Ni loadings of ca. 40 wt %. To alter the Ni particle size, the calcination temperature was varied from 400 to 800 °C, which led to gradual growth of Ni particles from 4.5 to 7.9 nm [as determined by transmission electron microscopy (TEM); Figure 2A] due to Ni sintering at higher treatment temperatures. The hydrogenolysis of 2-phenylethyl phenyl ether (β-O-4) was conducted over these five Ni/SiO$_2$ catalysts at 120 °C with 6 bar H$_2$ for 90 min in the aqueous phase. The results consistently showed that almost equal concentrations of C$_6$ (phenol, cyclohexanone, and cyclohexanol) and C$_8$ (ethylbenzene) compounds were formed under the selected conditions (Table 1). The C−O bond cleavage rate normalized to accessible Ni atoms [i.e., the turnover frequency (TOF)] first increased from 7 to 12, 17, and 26 h^{-1} as the Ni particle size increased from 4.5 to 4.7, 5.4, and 5.9 nm, respectively, and then dropped to 20 h^{-1} with a further increase in particle size to 8 nm (Figure 2B). To obtain the best compromise between optimum catalytic stability and activity, we selected a catalyst with larger particles for the in-depth study. The Ni/SiO$_2$ catalyst (57 wt % Ni loading) had a Brunauer−Emmett−Teller (BET) surface area of 140 m^2·g^{-1} with a pore volume of 0.1826 cm^3·g^{-1} and a particle size of ca. 3 μm as determined by scanning electron microscopy (SEM). The supported Ni particles had an average particle diameter of 8.0 ± 1.8 nm as determined by TEM, and the atomic fraction of Ni available for catalysis was 5% as measured by H$_2$ chemisorption (see the Supporting Information).

Kinetics of 2-Phenylethyl Phenyl Ether (β-O-4) Conversion. Figure 3a shows the product distribution for 2-phenylethyl phenyl ether (β-O-4) conversion as a function of time at 120 °C in the presence of 6 bar H$_2$. Cyclohexanol and ethylbenzene were the major products at reaction time $t = 0$, each being obtained with 50% selectivity during the conversion. Phenol was hardly detected because it was completely hydrogenated to cyclohexanol, while ethylbenzene remained nearly unconverted over Ni/SiO$_2$, with the selectivity for

ethylcyclohexane being lower than 2%. The selectivity for hydrogenated single-aromatic-ring products was below 2% independent of the conversion. The C−O−C bond was selectively cleaved at the position of the aliphatic carbon, producing phenol and ethylbenzene (Figure 3b). The selectivity for benzene and 2-phenylethanol was less than 1% even after 600 min. This indicates a preferred interaction of the aliphatic C−O bond in 2-phenylethyl phenyl ether (β-O-4) on the Ni surface. In summary, hydrogenolysis is the dominant reaction pathway for cleavage of 2-phenylethyl phenyl ether (β-O-4) with Ni/SiO$_2$ in the aqueous phase, affording ethylbenzene and phenol as the primary products (Figure 3b).

This result also highlights the importance of the hydroxyl group of phenol for adsorption on Ni/SiO$_2$ as well as the different solubilities of phenol (8.3 g/100 mL of H$_2$O at 20 °C) and ethylbenzene (0.018 g/100 mL of H$_2$O at 20 °C) in hot water. Separate experiments showed that the rate of phenol hydrogenation over Ni/SiO$_2$ (130 mol·mol$_{Ni(surf)}^{-1}$·h^{-1}) was 2 orders of magnitude higher than that of ethylbenzene (0.8 mol·mol$_{Ni(surf)}^{-1}$·h^{-1}) in water (Table 2). In nonpolar

Table 2. Hydrogenation of Aromatic Compounds on Ni/SiO$_2$ in the Aqueous Phase at 120 °C[a]

entry	reactant	solvent	catalyst amount (g)	conv. (%)	TOF (h^{-1})
1	phenol	water	0.03	15	130
2	phenol + ethylbenzene	water	0.03	20[b]	173[b]
				0[c]	0[c]
3	phenol	hexadecane	0.03	10	87
4	ethylbenzene	hexadecane	0.3	16	13
5	benzene	water	0.3	3.4	2.9
6	toluene	water	0.3	2.1	1.8
7	ethylbenzene	water	0.3	1.0	0.8

[a]Reaction conditions: reactant (0.010 mol), H$_2$O (80 mL), 6 bar H$_2$, 50 min, stirring at 700 rpm. [b]For phenol. [c]For ethylbenzene.

hexadecane, the rate of phenol hydrogenation (87 mol·mol$_{Ni(surf)}^{-1}$·h^{-1}) was lower than that in water (130 mol·mol$_{Ni(surf)}^{-1}$·h^{-1}) at 120 °C because of the difference in the solubilities of the reactant. The ethylbenzene hydrogenation rate in hexadecane (13 mol·mol$_{Ni(surf)}^{-1}$·h^{-1}) was still lower than that of phenol (87 mol·mol$_{Ni(surf)}^{-1}$·h^{-1}), indicating that the increased capability for adsorption on Ni/SiO$_2$ due to the phenol hydroxyl group plays a more significant role than the
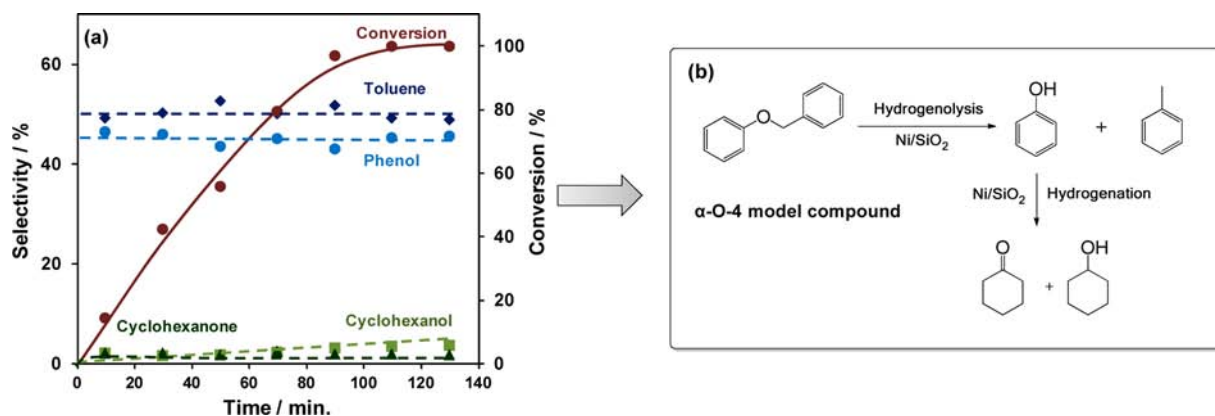
Figure 4. (a) Product distributions for the conversion of benzyl phenyl ether (α-O-4) over Ni/SiO$_2$ as functions of time. Reaction conditions: benzyl phenyl ether (α-O-4) (1.84 g, 0.010 mol), 57 wt % Ni/SiO$_2$ (0.030 g, 2.91 × 10^{-4} mol of Ni), H$_2$O (80 mL), 120 °C, 6 bar H$_2$, stirring at 700 rpm. (b) Reaction pathway for the cleavage of benzyl phenyl ether (the model for α-O-4 bond linkage in lignin) over Ni/SiO$_2$ in the aqueous phase.
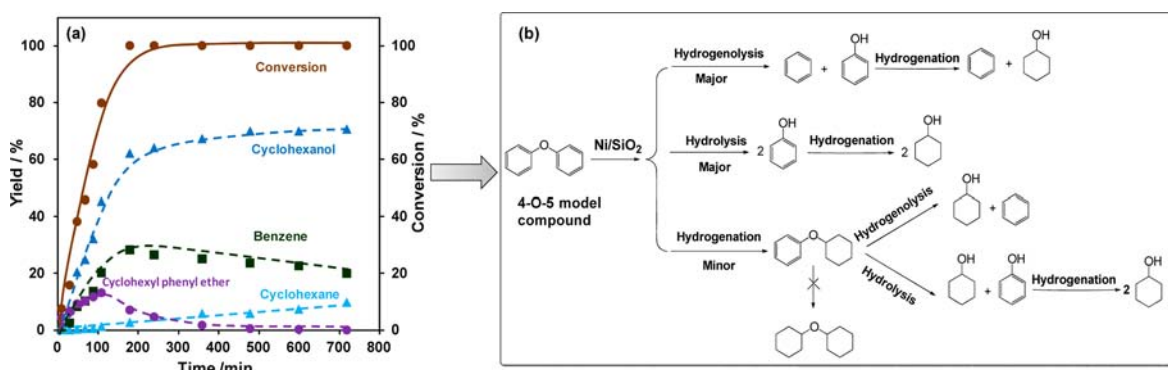

Figure 5. (a) Product distributions for the conversion of diphenyl ether (4-O-5) over Ni/SiO$_2$ as functions of time. Reaction conditions: diphenyl ether (4-O-5) (1.70 g, 0.010 mol), 57 wt % Ni/SiO$_2$ (0.30 g, 2.91 × 10^{-3} mol of Ni), 120 °C, 6 bar H$_2$, stirring at 700 rpm. (b) Reaction pathway for the cleavage of diphenyl ether (the model for the 4-O-5 linkage in lignin) over Ni/SiO$_2$ in the aqueous phase.

solvent. When phenol and ethylbenzene were added as *co*-reactants in water, ethylbenzene was unconverted, but phenol achieved a high hydrogenation rate with a TOF of 173 mol·mol$_{Ni(surf)}^{-1}$·h^{-1}. These results show that phenol is highly reactive whereas ethylbenzene hardly reacts at all on Ni/SiO$_2$ under the selected conditions.

Kinetics of Benzyl Phenyl Ether (α-O-4) Conversion. The reaction of benzyl phenyl ether (α-O-4) on Ni/SiO$_2$ at 120 °C with 6 bar H$_2$ (Figure 4a) showed a very high reaction rate, even in the presence of only a tenth of the catalyst used for 2-phenylethyl phenyl ether (β-O-4) conversion. The initial TOF for the C−O cleavage (1017 mol·mol$_{Ni(surf)}^{-1}$·h^{-1}) was much higher than that for the β-O-4 bond (13 mol·mol$_{Ni(surf)}^{-1}$·h^{-1}) (Table 4). The results agree well with the reports that the α-O-4 bond is thermally very unstable.[12] The primary products were toluene and phenol, each of which was obtained with nearly 50% selectivity at t = 0; as above, these products resulted from direct hydrogenolysis of the aliphatic C−O bond of benzyl phenyl ether.
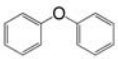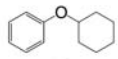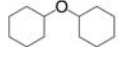
The phenol hydrogenation rate (130 mol·mol$_{Ni(surf)}^{-1}$·h^{-1}) was much higher than that of toluene (1.8 mol·mol$_{Ni(surf)}^{-1}$·h^{-1}) (Table 2). The very low catalyst concentration, however, was sufficient to catalyze the ether hydrogenolysis effectively but not the hydrogenation of the phenol aromatic ring. When the catalyst concentration was increased to that used for the β-O-4 conversion (0.30 g), 46% selectivity for toluene and 54% selectivity for cyclohexanol at 93% conversion was observed within 50 min. In summary, the reaction pathway for benzyl

phenyl ether (α-O-4) conversion using Ni/SiO$_2$ in the aqueous phase is dominated by the hydrogenolysis of benzyl phenyl ether to toluene and phenol, which is followed by a small extent of hydrogenation of phenol to cyclohexanone and cyclohexanol (Figure 4b).

Kinetics of Diphenyl Ether (4-O-5) Conversion. The conversion of diaryl ethers has been reported to be challenging, requiring severe conditions such as hydrolysis in supercritical water to cleave the C−O bond.[8] The C−O bond was also cleaved with Raney Ni in boiling methanol, but the achieved rate was extremely low (0.01 mol·mol$_{Ni}^{-1}$·h^{-1}).[13] Diphenyl ether (4-O-5) was reacted under the same conditions as reported above for β-O-4 (Figure 5a). The major products were cyclohexanol (25% selectivity), benzene (10% selectivity), and cyclohexyl phenyl ether (65% selectivity) at t = 0, suggesting a different reaction mechanism than for α-O-4 and β-O-4, in which hydrogenolysis and hydrogenation were sequential. As the reaction proceeded, the yields of cyclohexanol and benzene increased steadily, and the yield of cyclohexyl phenyl ether first increased to a maximum of 13% and then decreased to zero. Cyclohexanol was formed from phenol at a high rate of 130 mol·mol$_{Ni(surf)}^{-1}$·h^{-1}, which was much faster than the rate of benzene hydrogenation (2.9 mol·mol$_{Ni(surf)}^{-1}$·h^{-1}) (Table 2). The increasing concentrations of phenol and benzene did not result from the hydrogenolysis of cyclohexyl phenyl ether, as a separate reaction with cyclohexyl phenyl ether over Ni/SiO$_2$ showed that the C−O bond cleavage rate was relatively low (0.8 mol·mol$_{Ni(surf)}^{-1}$·h^{-1}), while dicyclohexyl ether did not

react under the conditions used (Table 3). The rate of diphenyl ether cleavage (26 mol·mol$_{Ni(surf)}^{-1}$·h^{-1}) was much higher, and we conclude that the hydrogenation/hydrogenolysis route is only a minor pathway (Figure 5b).

Table 3. Rates of C−O Bond Cleavage in Diphenyl Ether (4-O-5), Cyclohexyl Phenyl Ether, and Dicyclohexyl Ether at 120 °C^a

Reactant	Selectivity (%)			Conv. (%)	Initial TOF (h^{-1})
	Benzene	Cyclohexanol	CPE^b		
(diphenyl ether)	27	57	16	80	26
(cyclohexyl phenyl ether)	32	68	-	2.1	0.8
(dicyclohexyl ether)	0	0	0	0	0

^{a}Reaction conditions: reactant (0.010 mol), 57 wt % Ni/SiO$_2$ (0.30 g, 2.91 × 10^{-3} mol of Ni), H$_2$O (80 mL), 6 bar H$_2$, 110 min, stirring at 700 rpm. ^{b}CPE = cyclohexyl phenyl ether.

The selectivity for cyclohexanol (70%) was 2.3 times higher than the selectivity for benzene (30%) at complete conversion. Considering that the selectivity for cyclohexanol (formed from phenol hydrogenation) was much higher than that for benzene, we therefore conclude that hydrolysis of diphenyl ether (4-O-5) occurred in parallel to hydrogenolysis, producing two molecules of phenol. Thus, cyclohexanol was obtained from diphenyl ether via two routes, one relying on sequential hydrolysis/hydrogenation and the other replying on sequential hydrogenolysis/hydrogenation (Figure 5b). It is estimated that the ratio of the hydrogenolysis rate to the hydrolysis rate is ca. 3:2.

In summary, the overall reaction pathway for diphenyl ether conversion (Figure 5b) follows two major routes: (i) hydrogenolysis of diphenyl ether to benzene and phenol, after which phenol is rapidly hydrogenated to cyclohexanol, and (ii) hydrolysis of diphenyl ether to two molecules of phenol, which in turn are hydrogenated to cyclohexanol. Another route of minor importance is the hydrogenation of diphenyl ether to cyclohexyl phenyl ether, which in turn is hydrolyzed or hydrogenolyzed to cyclohexanol, benzene, and phenol. Phenol is in turn hydrogenated to cyclohexanol, and a small fraction of benzene is hydrogenated to cyclohexane.
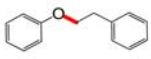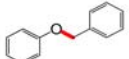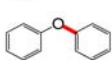
Relation of the Thermodynamic Properties of the Reactant to the Kinetic Parameters. After exploring the differences in the kinetic behavior of the three model compounds on Ni/SiO$_2$, we next explored how the strength of the ether bond, characterized by the bond dissociation energy (BDE),[14] correlates with the kinetic parameters (Table 4). The aryl ether bond (BDE = 314 kJ·mol^{-1}) of 4-O-5 is much stronger than the aliphatic ether bonds of α-O-4 (218 kJ·mol^{-1}) and β-O-4 (289 kJ·mol^{-1}). Thus, hydrogenolysis favors selective cleavage of the weaker aliphatic ether bonds. The aliphatic ether C−O bond of α-O-4 is weaker than the aryl ether C−O bond of 4-O-5 by 96 kJ·mol^{-1} and is more easily cleaved under hydrothermal conditions above 250 °C even in a blank test (see Figure S6 in the Supporting Information). The low BDE of α-O-4 (218 kJ·mol^{-1}) leads to a very high initial TOF (1017 mol·mol$_{Ni(surf)}^{-1}$·h^{-1}) and a lower apparent activation energy (E_a = 72 kJ·mol^{-1}), as determined from an Arrhenius plot (Figure 6a). By comparison, the higher BDE of the aliphatic ether bond of β-O-4 (289 kJ·mol^{-1}) leads to a low TOF (13 mol·mol$_{Ni(surf)}^{-1}$·h^{-1}) and a much higher E_a (86 kJ·mol^{-1}) (Figure 6a).

Relative to α-O-4 and β-O-4, 4-O-5 showed very different reactivity on Ni/SiO$_2$. In principle, the C−O bond of the 4-O-5 linkage should be the most difficult ether bond to cleave, as it has the highest BDE (314 kJ·mol^{-1}). Previous work would also support this conclusion.[8,11] The fact that 4-O-5 has the highest E_a (97 kJ·mol^{-1}) agrees with the fact that it has the highest BDE. However, the reaction rate for 4-O-5 (26 mol·mol$_{Ni(surf)}^{-1}$·h^{-1}) was significantly higher than that for β-O-4 (13 mol·mol$_{Ni(surf)}^{-1}$·h^{-1}) with the Ni/SiO$_2$ catalysts. This may be attributed to the different C−O bond cleavage mechanisms for 4-O-5 and β-O-4. The C−O bonds in benzyl phenyl ether (α-O-4) and 2-phenylethyl phenyl ether (β-O-4) were directly cleaved by Ni catalyzed hydrogenolysis. However, the C−O bond of 4-O-5 was cleaved by parallel hydrogenolysis and hydrolysis, in which hydrolysis appears to increase the overall conversion rate. It should be noted that the apparent activation energies for cleavage of α-O-4, β-O-4, and 4-O-5 increased almost linearly with their C−O BDEs (Figure 6b), indicating that the aryl C−O bond cleavage barrier is heavily influenced by the C−O BDE.

To explore the specific contributions of the Ni/SiO$_2$ components in water, the C−O cleavage rates for the three model compounds were compared with those in pure water, with SiO$_2$, and with Ni/SiO$_2$ in the presence of 6 bar H$_2$ at 120 °C (Table 4). None of the ethers reacted in pure water or in the presence of SiO$_2$ alone. With the Ni/SiO$_2$ catalyst, the C−

Table 4. Bond Dissociation Energies (BDEs), Initial Turnover Frequencies (TOFs) of C−O Cleavage, and Apparent Activation Energies (E_a) for C−O Bond Cleavage in Lignin Model Compounds

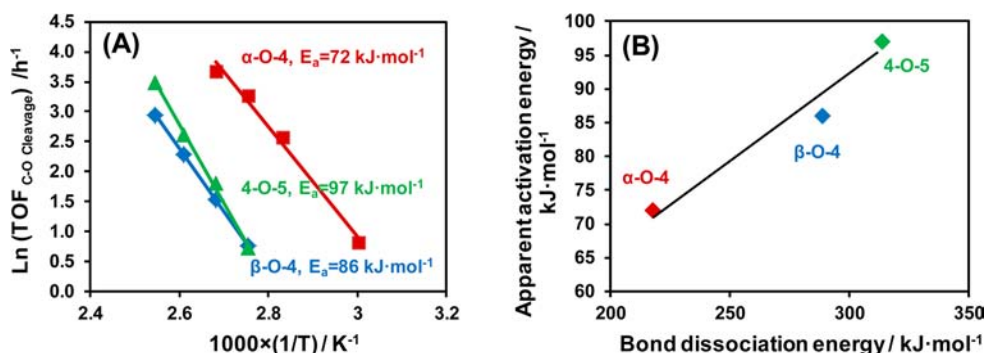| Linkage	Model Compound	BDE (kJ·mol^{-1})^a	E_a (kJ·mol^{-1})	TOF$_{Ni/SiO_2}$ (h^{-1})	TOF$_{H_2O}$ (h^{-1})	TOF$_{SiO2}$ (h^{-1})
β-O-4		289	86	13	0	0
α-O-4		218	72	1017	0	0
4-O-5		314	97	26	0	0

^{a}Data from ref 14.

Figure 6. (a) Arrhenius plots [ln(TOF) vs $1/T$] for the three model compounds. Reaction conditions: H_2O (80 mL); 6 bar H_2; 50 min; and either (i) α-O-4 (1.84 g), 57 wt % Ni/SiO_2 (0.03 g, 2.91×10^{-4} mol of Ni); (ii) β-O-4 (1.98 g), 57 wt % Ni/SiO_2 (0.30 g, 2.91×10^{-4} mol of Ni); or (iii) 4-O-5 (1.70 g), 57 wt % Ni/SiO_2 (0.30 g, 2.91×10^{-4} mol of Ni). (b) Relationship between apparent E_a and BDE for the three model compounds.

O bond cleavage rates for α-O-4 (1017 mol·$mol_{Ni(surf)}^{-1}$·h^{-1}), β-O-4 (13 mol·$mol_{Ni(surf)}^{-1}$·h^{-1}), and 4-O-5 (26 mol·$mol_{Ni(surf)}^{-1}$·h^{-1}) increased dramatically, verifying that the Ni center is the active site for C−O bond cleavage.

Impact of the H_2 Pressure. The product distributions for the β-O-4, α-O-4, and 4-O-5 model compounds were recorded at conversions lower than 15% over Ni/SiO_2 at 120 °C with varying H_2 pressure (Figures S7−S9 in the Supporting Information). In the absence of H_2, none of the model compounds reacted. Thus, the presence H_2 is also required for the hydrolysis route of diphenyl ether (4-O-5). With increasing P_{H_2}, the rates of C−O bond cleavage in β-O-4 and 4-O-5 first increased to maxima at 6 and 10 bar H_2, respectively, and then gradually decreased (Figure 7). The C−O bond cleavage on Ni
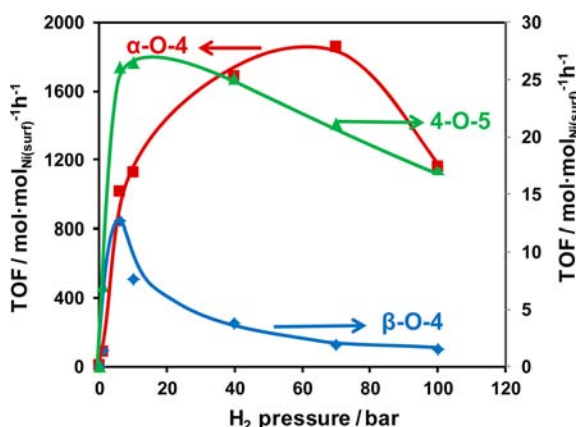

Figure 7. TOFs for the three model compounds over Ni/SiO_2 as functions of H_2 pressure. Detailed conditions are given in the Supporting Information.

is the rate-determining step,[15] so these results suggest that H_2 competes with the organic reactant for adsorption sites. Up to medium P_{H_2}, the increasing surface coverage leads to an increased hydrogenolysis rate, while at high P_{H_2}, the rate is retarded because of the lower ether coverage.[16] Thus, Figure 7 represents a typical change in the hydrogenolysis rate for β-O-4 and 4-O-5.

In contrast, the rate of C−O bond cleavage for α-O-4 increased with P_{H_2} up to 80 bar. This is attributed to the fact that Ni/SiO_2 leads to a much higher rate of C−O bond cleavage in α-O-4, with the maximum cleavage rate being 150 and 70 times faster than those for α-O-4 and 4-O-5,

respectively (Figure 7). This causes product desorption to be rate-determining at lower P_{H_2}, and a higher H_2 pressure facilitates product removal via hydrogen addition and hydrogen-aided desorption. When P_{H_2} was increased to 100 bar, the TOF for C−O bond cleavage of α-O-4 decreased because of the decrease in reactant coverage derived from the competition between reactant and H_2 for adsorption on the Ni sites. Variation of the H_2 pressure also led to differences in the hydrogenation pathways of the model compounds. With increasing P_{H_2}, the selectivity for hydrogenated single-aromatic-ring products increased from 0 to 45 and 20% for β-O-4 and 4-O-5, respectively (Figures S7 and S9 in the Supporting Information). However, a hydrogenated single-aromatic-ring product was not observed for α-O-4 even at 100 bar H_2 (Figure S8 in the Supporting Information). This implies the following: (i) Hydrogenolysis and hydrogenation are competing reactions, and higher H_2 pressure favors the hydrogenation of a single aromatic ring of 4-O-5 and β-O-4. (ii) α-O-4 shows a different behavior because its hydrogenolysis barrier (72 kJ·mol^{-1}) is much lower than the E_a for hydrogenation of the phenolic ring over Ni/SiO_2 (ca. 100 kJ·mol^{-1}),[17] and therefore, hydrogenolysis dominates over hydrogenation at low temperatures.

Comparison of the Mechanisms of C−O Bond Cleavage for the Three Model Compounds. On the basis of the above results and discussion, the α-O-4 and β-O-4 $C_{aliphatic}$−O−$C_{aromatic}$ linkages are cleaved on the $C_{aliphatic}$−O side by the Ni-catalyzed hydrogenolysis. However, for 4-O-5, the $C_{aromatic}$−O−$C_{aromatic}$ linkage is cleaved by hydrogenolysis and hydrolysis in parallel. It has been shown that hydrolysis of the 4-O-5 linkage does not occur in the absence of H_2 (Figure 7) or Ni/SiO_2 (Table 4). Hydrolysis is hypothesized to occur along the same reaction path as hydrogenolysis, with cleavage by Ni and subsequent addition of H· and OH· (from water dissociation) instead of addition of two H· (Figure 8B). For the α-O-4 and β-O-4 compounds, the weaker $C_{aliphatic}$−O bonds rather than the stronger $C_{aromatic}$−O bonds are cleaved (Figure 8A). As the BDE of the $C_{aliphatic}$−O bond in the α-O-4 linkage (218 kJ·mol^{-1}) is much lower than that in the β-O-4 linkage (289 kJ·mol^{-1}), the rate of hydrogenolysis of the α-O-4 linkage over Ni/SiO_2 is 2 orders of magnitude higher than that of β-O-4 linkage (Table 4).

Once the $C_{aliphatic}$−O bonds in the α-O-4 and β-O-4 linkages are cleaved into $C_{aliphatic}$· and ·O−$C_{aromatic}$ fragments, the abundant dissociated H· atoms on the Ni surface are in turn added to form methyl- or ethylbenzene, respectively, and
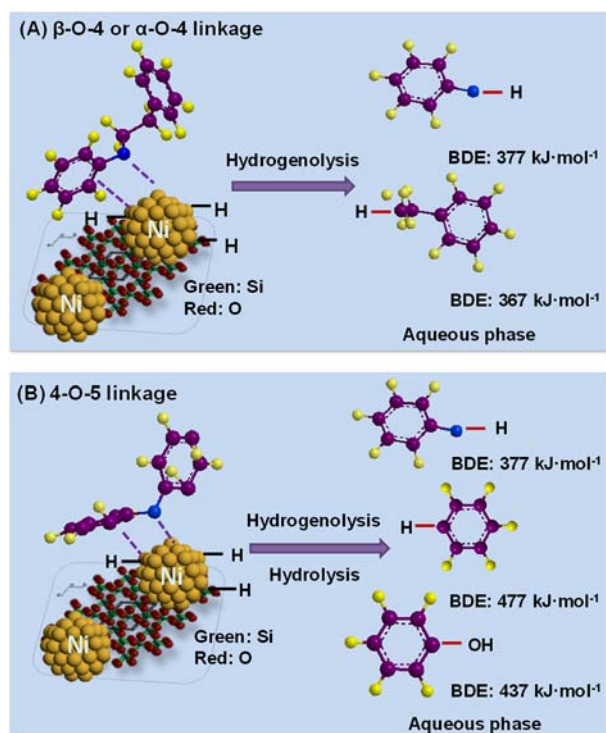
Figure 8. Proposed mechanisms for cleavage of C–O bonds in the α-O-4, β-O-4, and 4-O-5 model compounds.

phenol (Figure 8A). As the BDEs of $PhCH_2CH_2$–H and $PhCH_2CH_2$–OH are 367 and 333 kJ·mol^{-1},[14a] respectively, it appears that $PhCH_2CH_2$· prefers to combine with H· but not OH· (from water dissociation) because of the much higher (by 34 kJ·mol^{-1}) bond formation energy for this process, which makes hydrogenolysis (H· addition) dominant. In addition, the BDE of Ph–H (477 kJ·mol^{-1}) is also much higher than that of Ph–OH (437 kJ·mol^{-1}),[14a] so hydrogenolysis rather than hydrolysis contributes a substantial fraction to the overall 4-O-5 conversion (Figure 5). In essence, hydrolysis combined with OH· and H· addition could occur on all three model compounds in water, but the low concentrations of $PhCH_2OH$ and $PhCH_2CH_2OH$ produced can be further hydrogenolyzed to $PhCH_3$ and $PhCH_2CH_3$, respectively (Table S1 in the Supporting Information), while hydrogenation to produce cyclohexanol is the major reaction of phenol derived from the 4-O-5 linkage under the present conditions (Table 2). Therefore, hydrogenolysis is the major reaction pathway for the overall conversions of the α-O-4 and β-O-4 linkages, and parallel hydrogenolysis/hydrolysis is the major route for conversion of the 4-O-5 linkage with Ni/SiO$_2$ catalysts in water.

CONCLUSION

The C–O bond linkages of α-O-4, β-O-4, and 4-O-5 model compounds representing typical bonds in lignin were selectively cleaved by a silica-supported Ni catalyst to produce aromatic and aliphatic molecules as well as cyclohexanol in aqueous media under mild conditions (120 °C, 6 bar H$_2$). The C–O bonds of α-O-4 and β-O-4 are cleaved by direct hydrogenolysis, which has been shown to be structure-sensitive on Ni-based catalysts, while the C–O bond of 4-O-5 appear to be cleaved by parallel hydrogenolysis and hydrolysis. The difference is attributed to the hydrogenolysis of the low concentrations of $PhCH_2OH$ and $PhCH_2CH_2OH$ intermediates from the α-O-4

and β-O-4 linkages to give $PhCH_3$ and $PhCH_2CH_3$, respectively, while hydrogenation converts phenol derived from the 4-O-5 linkage to cyclohexanol under the present conditions.

The rates for C–O bond cleavage decreased in the order (α-O-4) > (4-O-5) > (β-O-4), and the apparent energies of activation increased in the order (α-O-4) < (β-O-4) < (4-O-5), tracking with the variation in the bond dissociation energies, (α-O-4) < (β-O-4) < (4-O-5). The C–O bond of 4-O-5 is cleaved by parallel hydrogenolysis and hydrolysis, and the additional hydrolysis route accelerates the conversion. In the hydrogenolysis of β-O-4 and 4-O-5, an optimal H$_2$ pressure maximized the reaction rates for C–O bond cleavage, because the organic reactant competes with H$_2$ for the active sites. In contrast, the rate of C–O bond cleavage increased continuously up to 80 bar for α-O-4 conversion, probably because increasing P_{H_2} facilitates product desorption from the Ni surface (the rate-determining step for α-O-4 at low P_{H_2}). As P_{H_2} is further increased, the TOF of C–O bond cleavage of α-O-4 decreases because of the lower reactant coverage resulting from the competition between reactant and H$_2$ adsorption on the Ni sites.

The results indicate that Ni-based solid catalysts are interesting and stable for ether cleavage and exhibit significantly higher rates than related molecular catalysts. Tailoring the Ni catalyst via variation of the particle size and eventually the support is expected to lead to a new group of catalysts for cleaving carbon–heteroatom bonds.

MATERIALS AND METHODS

Materials. The chemicals were purchased from commercial suppliers and used as provided: benzyl phenyl ether (TCI, >98% GC assay), 2-phenylethyl phenyl ether (Frinton Laboratories, >99% GC assay), diphenyl ether (Sigma-Aldrich, >99% GC assay), cyclohexyl phenyl ether (Sigma-Aldrich, >95% GC assay), benzene (Fluka, >99.5% GC assay), toluene (Sigma-Aldrich, >99.5% GC assay), ethylbenzene (Fluka, >99% GC assay), phenol (Sigma-Aldrich, >99% GC assay), ethyl acetate (Sigma-Aldrich, >99.5% GC assay), nickel(II) nitrate hexahydrate (Sigma-Aldrich, ≥98.5%), urea (Sigma-Aldrich, BioReagent), HNO$_3$ (Sigma-Aldrich, >65%), 5 wt % Pd/C (Sigma-Aldrich), SiO$_2$ (Aerosil 200, Evonik-Degussa), H$_2$ (Air Liquide, >99.999%), N$_2$ (Air Liquide, > 99.999%).

Ni/SiO$_2$ Catalyst Preparation Using the DP Method. An aqueous solution (250 mL) containing Ni(NO$_3$)$_2$·6H$_2$O (0.14 M, 10.2 g) was divided in two parts. To one part (50 mL) was added urea (0.42 M, 6.3 g), and the other part (200 mL) together with SiO$_2$ (1.9 g) and HNO$_3$ (65%, 0.02 M, 0.32 mL) was put into a flask thermostatted at 80 °C. The urea solution was then slowly added to the flask, and the suspension was rapidly heated to 90 °C, after which the suspension was magnetically stirred for 10 h. The suspension was then cooled to 25 °C, and the solids were filtered and washed three times with distilled water (5/1 water/slurry). Finally, the sample was dried at 90 °C for 24 h; calcined in flowing air (100 mL·min^{-1}) at 400, 500, 600, 700, or 800 °C; and reduced in flowing H$_2$ (100 mL·min^{-1}) at 460 °C.

Catalytic Test. The detailed reaction conditions are described in the figure captions and table footnotes. In a typical experiment, the catalytic reactions were carried out in a slurry autoclave reactor loaded with Ni/SiO$_2$ using water as the solvent at 120 °C in the presence of 6 bar H$_2$. The lignin model compound (0.010 mol), 57 wt % Ni/SiO$_2$ (0.30 g, 2.91 × 10^{-3} mol of Ni for β-O-4 and 4-O-5 or 0.030 g, 2.91 × 10^{-4} mol of Ni for α-O-4), and H$_2$O (80 mL) were charged into a Parr reactor (Series 4848, 300 mL). After the reactor was flushed with H$_2$ three times, the autoclave was charged with 6 bar H$_2$, and the reaction was conducted at 120 °C with a stirring speed of 700 rpm. Because it is a two-phase reaction, the kinetic data were collected at time durations.

After the reaction, the reactor was quenched to ambient temperature using ice, and the organic products were extracted using ethyl acetate and analyzed by gas chromatography (GC) and GC−mass spectroscopy (GC−MS) analysis on a Shimadzu 2010 gas chromatograph with flame ionization detector and a Shimadzu QP 2010S GC−MS instrument, both equipped with HP-5 capillary columns (30 m × 250 μm). 2-Isopropylphenol was used as an internal standard to calibrate the liquid product concentrations and carbon balances. The carbon balances for all of the reported experiments were better than 95 ± 3%. The calculations of conversion and selectivity were on a carbon mole basis. Conversion is defined as the amount of change in raw materials during the reaction divided by the total amount of starting material, multiplied by 100%. The selectivity is defined as the number of C atoms in the product of interest divided by the total number of C atoms in the products, multiplied by 100%.

Catalyst Characterization. *Atomic Absorption Spectroscopy.* A UNICAM 939 atomic absorption spectrometer was used to determine the concentration of nickel in Ni/SiO$_2$. Before measurement, a mixture of 0.5 mL of 48 wt % hydrofluoric acid and 0.1 mL of nitrohydrochloric acid was used to dissolve 20−40 mg of the sample at 383 K (the boiling point of the mixture).

NMR Spectroscopy. The ^{1}H, ^{13}C, and correlation spectroscopy (COSY) NMR measurements were performed on a JEOL 400 MHz spectrometer. CDCl$_3$ was used as the solvent.

BET Analysis. The BET surface areas and pore diameters were determined from N$_2$ adsorption measurements carried out at 77 K on a PMI automated BET sorptometer. The samples were outgassed at 523 K for 20 h before measurement.

H$_2$ Chemisorption. The catalysts were activated at 733 K for 3 h in H$_2$ and 1 h in vacuum and then cooled to 313 K. H$_2$ adsorption (chemisorption and physisorption) was then measured over the pressure range from 1 to 40 kPa. Next, the physisorbed H$_2$ was removed by outgassing the sample at the same temperature for 1 h, and another isotherm (physisorption) was measured. The concentration of chemisorbed hydrogen on the metal was determined by extrapolating the differential isotherm to zero H$_2$ pressure, and this value was used to calculate the Ni dispersion.

Transmission Electron Microscopy. TEM images were measured on a JEOL JEM-2010 transmission electron microscope operating at 120 kV. Before measurement, the catalyst was ground, suspended in ethanol, and dispersed by ultrasonic treatment. The obtained dispersion was transferred to a copper-grid-supported carbon film. TEM images were recorded with a magnification of 200 000. The average cluster size was calculated by counting 300 metal particles.

Scanning Electron Microscopy. SEM images were recorded on a JEOL REM 5900 LV microscope operating at 25 kV. The powder samples were used without any pretreatment.

■ ASSOCIATED CONTENT

Ⓢ Supporting Information

SEM and TEM images of the catalyst; synthesis and ^{1}H, ^{13}C, and COSY NMR characterization of dicyclohexyl ether; product yields for the conversion of benzyl phenyl ether in the absence of H$_2$; and product distributions with varying H$_2$ pressure. This material is available free of charge via the Internet at http://pubs.acs.org.

■ AUTHOR INFORMATION

Corresponding Author

chenzhao@mytum.de; johannes.lercher@ch.tum.de.

Notes

The authors declare no competing financial interest.

■ ACKNOWLEDGMENTS

■ REFERENCES

(1) Stöcker, M. *Angew. Chem., Int. Ed.* **2008**, *47*, 9200−9211.
(2) (a) Regalbuto, J. R. *Science* **2009**, *325*, 822−824. (b) Perlack, R. D.; Wright, L. L.; Turhollow, A. F.; Graham, R. L.; Stokes, B. J.; Erbach, D. C. *Biomass as Feedstock for a Bioenergy and Bioproducts Industry: The Technical Feasibility of a Billion-Ton Annual Supply*; U.S. Department of Energy: Washington, DC, **2005**. (c) Huber, G. W.; Corma, A. *Angew. Chem., Int. Ed.* **2007**, *46*, 7184−7201. (d) Huber, G. W.; Iborra, S.; Corma, A. *Chem. Rev.* **2006**, *106*, 4044−4098.
(3) (a) Ragauskas, A. J.; Williams, C. K.; Davison, B. H.; Britovsek, G.; Cairney, J.; Eckert, C. A.; Frederick, W. J., Jr.; Hallett, J. P.; Leak, D. J.; Liotta, C. L.; Mielenz, J. R.; Murphy, R.; Templer, R.; Tschaplinski, T. *Science* **2006**, *311*, 484−489. (b) Chang, M. C. Y. *Curr. Opin. Chem. Biol.* **2007**, *11*, 677−684. (c) Sanderson, K. *Nature* **2011**, *474*, S12−S14. (d) Matson, T. D.; Barta, K.; Iretskii, A. V.; Ford, P. C. *J. Am. Chem. Soc.* **2011**, *133*, 14090−14097.
(4) Nichols, J. M.; Bisshop, L. M.; Bergman, R. G.; Ellman, J. A. *J. Am. Chem. Soc.* **2010**, *132*, 12554−12555.
(5) Son, S.; Toste, F. D. *Angew. Chem., Int. Ed.* **2010**, *49*, 3791−3794.
(6) Sergeev, A. G.; Hartwig, J. F. *Science* **2011**, *332*, 439−443.
(7) (a) Roberts, V. M.; Knapp, R. T.; Li, X.; Lercher, J. A. *ChemCatChem* **2010**, *2*, 1407−1410. (b) Roberts, V. M.; Stein, V.; Reiner, T.; Li, X.; Lemonidou, A.; Li, X.; Lercher, J. A. *Chem—Eur. J.* **2011**, *17*, 5939−5948. (c) Roberts, V. M.; Fendt, S.; Reiner, T.; Li, X.; Lemonidou, A. A.; Li, X.; Lercher, J. A. *Appl. Catal., B* **2010**, *95*, 71−77.
(8) Zhao, C.; Lercher, J. A. *Angew. Chem., Int. Ed.* **2012**, *51*, 5935−5941.
(9) Zhao, C.; Lercher, J. A. *ChemCatChem* **2012**, *4*, 64−68.
(10) (a) Zakzeski, J.; Bruijnincx, P. C. A.; Jongerius, A. L.; Weckhuysen, B. M. *Chem. Rev.* **2010**, *110*, 3552−3599. (b) Furimsky, E. *Appl. Catal., A* **2000**, *199*, 147−190.
(11) (a) Zhao, C.; Kou, Y.; Lemonidou, A. A.; Li, X.; Lercher, J. A. *Chem. Commun.* **2010**, *46*, 412−414. (b) Zhao, C.; Kou, Y.; Lemonidou, A. A.; Li, X.; Lercher, J. A. *Angew. Chem., Int. Ed.* **2009**, *48*, 3987−3990. (c) Zhao, C.; Camaioni, D. M.; Lercher, J. A. *J. Catal.* **2012**, *288*, 92−103. (d) Zhao, C.; He, J.; Lemonidou, A. A.; Li, X.; Lercher, J. A. *J. Catal.* **2011**, *280*, 8−16. (e) Zhao, C.; Kazacov, S.; He, J.; Lercher, J. A. *J. Catal.* **2012**, *296*, 12−23. (f) Zhao, C.; Song, W.; Lercher, J. A. *ACS Catal.* **2012**, *2*, 2714−2723.
(12) (a) Dorrestijn, E.; Laarhoven, L.; Arends, I.; Mulder, P. *J. Anal. Appl. Pyrolysis* **2000**, *54*, 153−192. (b) Rylander, P. N. *Hydrogenation Methods*; Academic Press: London, 1985; pp 157−163.
(13) Chandler, G.; Sasse, W. *Aust. J. Chem.* **1963**, *16*, 20−30.
(14) (a) Luo, Y. R. In *Comprehensive Handbook of Chemical Bond Energies*; CRC Press: Boca Raton, FL, 2007. (b) Jarvis, M. W.; Daily, J. W.; Carstensen, H.; Dean, A. M.; Sharma, S.; Dayton, D. C.; Robichaud, D. J.; Nimlos, M. R. *J. Phys. Chem. A* **2011**, *115*, 428−438.
(15) Shang, S. B.; Kenney, C. N. *J. Catal.* **1992**, *134*, 134−150.
(16) Bond, G. C.; Cunningham, R. H. *J. Catal.* **1997**, *166*, 172−185.
(17) Hichri, H.; Accary, A.; Andrieu, J. *Chem. Eng. Process.* **1991**, *30*, 133−140.